Journal of Constructional Steel Research 186 (2021) 106898

Contents lists available at ScienceDirect

Journal of Constructional Steel Research

journal homepage: www.elsevier.com/locate/jcsr

Experimental investigation of direct-formed square and rectangular hollow section beams

Kamran Tayyebi [a], Min Sun [a,*], Kian Karimi [b], Ray Daxon [b], Brandon Rossi [b]

[a] Department of Civil Engineering, University of Victoria, Victoria, British Columbia V8P 5C2, Canada
[b] Department of Civil Engineering, British Columbia Institute of Technology, Vancouver, British Columbia V5G 3H2, Canada

ARTICLE INFO

Keywords:
Rectangular hollow section
Flexural design
Direct forming
Galvanizing
High-strength steel
Cross-section classification

ABSTRACT

This paper presents an experimental study on the flexural behaviours of new-generation direct-formed square and rectangular hollow sections (collectively referred to as RHS herein). A total of 22 beam specimens covering wide ranges of cross-sectional dimensions and nominal yield stresses (350 and 690 MPa) are tested. The results are compared to those from previously tested indirect-formed and hot-finished RHS to study the effect of different production processes. The effects of post-production hot-dip galvanizing on residual stresses and flexural behaviours are also studied. The applicability of slenderness limits and flexural design formulae in the current North American steel design standards are examined using the experimental data. The experimental results demonstrate that the existing flexural design rules are generally conservative for direct-formed RHS (ungalvanized and galvanized).

1. Introduction

In practice, cold-formed square and rectangular hollow sections (collectively referred to as RHS herein) with commonly specified cross-sectional dimensions are produced in North America using either the indirect-forming or the direct-forming approach (Fig. 1). The indirect-forming approach, as the conventional approach of the two, gradually roll-forms steel coil into a circular hollow section (CHS) before further shaping it into the desired rectangular shape. The direct-forming approach, as the new approach of the two, roll-forms steel coil directly into the final rectangular shape. In both approaches, the sections are closed using electric resistance welding (ERW). The design provisions for RHS members in the existing North American steel design standards (AISC 360–16 [1] and CSA S16–19 [2]) are in general developed based on research on indirect-formed RHS, and currently do not differentiate RHS cold-formed by different methods [3–5].

Recent research involving measurement of residual stresses in 26 RHS specimens with different production histories [3] showed that, comparing to indirect-formed RHS, direct-formed RHS in general have lower levels of residual stresses since the cold-working is mainly concentrated at the four corner regions during production. A complementary experimental investigation involving testing of 36 stub columns [4] showed that direct-formed RHS often have superior stub column behaviours than their indirect-formed counterparts. By comparing the failure modes and load carrying capacities of the stub column specimens to the predictions by the existing North American steel design standards [1,2], the current slenderness limits for compression elements in RHS subject to axial compression are shown to be excessively conservative for direct-formed RHS due to the inherently low levels of residual stresses. In many cases, the existing slenderness limits in [1,2] misjudged nonslender direct-formed sections as slender sections, resulting in unnecessary penalty to effective cross-sectional area. The existing design formulae in [1,2] for members under axial compression are found to be very conservative since they are derived heavily based on the existing slenderness limits. To address this practical design issue, [5] performed a subsequent finite element (FE) parametric investigation and proposed modified design recommendations for direct-formed RHS stub columns against cross-sectional yielding and local buckling. One of the primary objectives of this research is to extend the above work to study the structural behaviours of direct-formed RHS under flexural loading.

Other than direct-formed regular-strength RHS (nominal yield strength = 350 MPa), direct-formed high-strength RHS (nominal yield strength = 690 MPa) produced to ASTM A1112 [6] are now available in the North American market. Such high-strength RHS are cold-formed using coil materials produced by a thermo-mechanically controlled process (TMCP). The new RHS have already been extensively used in the

* Corresponding author.
E-mail address: msun@uvic.ca (M. Sun).

https://doi.org/10.1016/j.jcsr.2021.106898
Received 20 May 2021; Received in revised form 3 August 2021; Accepted 4 August 2021

Nomenclatures

B	External width
b	Flat width
b_e	Effective flange flat width
c_1, c_2	Imperfection adjustment factors in AISC 360–16
D_l	Average of deflections at two loading points
D_m	Deflection at mid-span
E	Young's modulus
f_u	Ultimate stress
f_y	Yield stress
H	External depth
h	Flat depth
L_m	Length of moment span
L_s	Length of shear span
$M_{n,\mathrm{AISC}}$	Nominal flexural strength based on ANSI/AISC 360–16
$M_{n,\mathrm{CSA}}$	Nominal flexural strength based on CSA S16–19
M_p	Plastic moment
M_u	Ultimate moment
M_y	Yield moment
R	Rotation capacity
r	Internal corner radius
S	Elastic section modulus
S_e	Effective section modulus
t	Wall thickness
Z	Plastic section modulus
ε_rup	Rupture strain from tensile coupon test
σ_b	Bending residual stress
σ_m	Membrane residual stress
κ_p	Elastic curvature corresponding to plastic moment
κ_u	Curvature at plastic moment during unloading
λ_{c1}, λ_{c2}, λ_{c3}	Class 1, 2 and 3 slenderness limits in CSA S16–19
λ_p	Plastic slenderness limit in AISC 360–16
λ_r	Yield slenderness limit in AISC 360–16

North American transportation and agricultural industries. However, their application in the building industry is limited. Previous research on high-strength RHS for building applications in general focuses on indirect-formed products [e.g., [7–15]]. On the other hand, research on direct-formed high-strength RHS is limited. Detailed literature review and discussions can be found in [3–5]. As the newest ASTM standard for cold-formed high-strength hollow structural sections, ASTM A1112 [6] currently does not appear as approved materials in [1,2] due to the lack of research. As the second objective of this research, the applicability of the existing flexural member design rules in [1,2] on direct-formed high-strength RHS is examined for the first time.

From power generation to transmission and distribution, the application of galvanized tubular steel structures covers nearly all fields of the energy infrastructure. To facilitate the application of galvanized high-strength hollow sections in durable energy infrastructure standing up to harsh environment and test of time, recent experimental research investigated the effect of post-production hot-dip galvanizing on residual stresses in cold-formed CHS [16] and RHS [3,17]. It was found that similar to the application of the heat treatment per ASTM A1085 Supplement S1 [18], or the Class H finish per CSA G40.20/G40.21 [19] (both at 450 °C), post-production hot-dip galvanizing can also effectively reduce the cold-forming-induced residual stresses. It should be noted that for hot-dip galvanizing, the molten zinc bath is typically maintained at 450 °C [20]. For batch galvanizing of hollow structural sections of commonly specified sizes, nearly the same steps are followed in all facilities. The immersion time for individual member is strictly controlled (approximately ten minutes) to produce the best coating quality [20]. It is therefore speculated that the application of post-production galvanizing will influence cold-formed RHS member behaviours under flexural loading. The third objective of this research is to substantiate this speculation.

In all, this paper presents an experimental investigation involving a total of 22 full-scale beam specimens to address the above research questions. The applicability of the existing slenderness limits for compression elements in RHS subject to flexure and the corresponding flexural design formulae in [1,2] for direct-formed regular- and high-

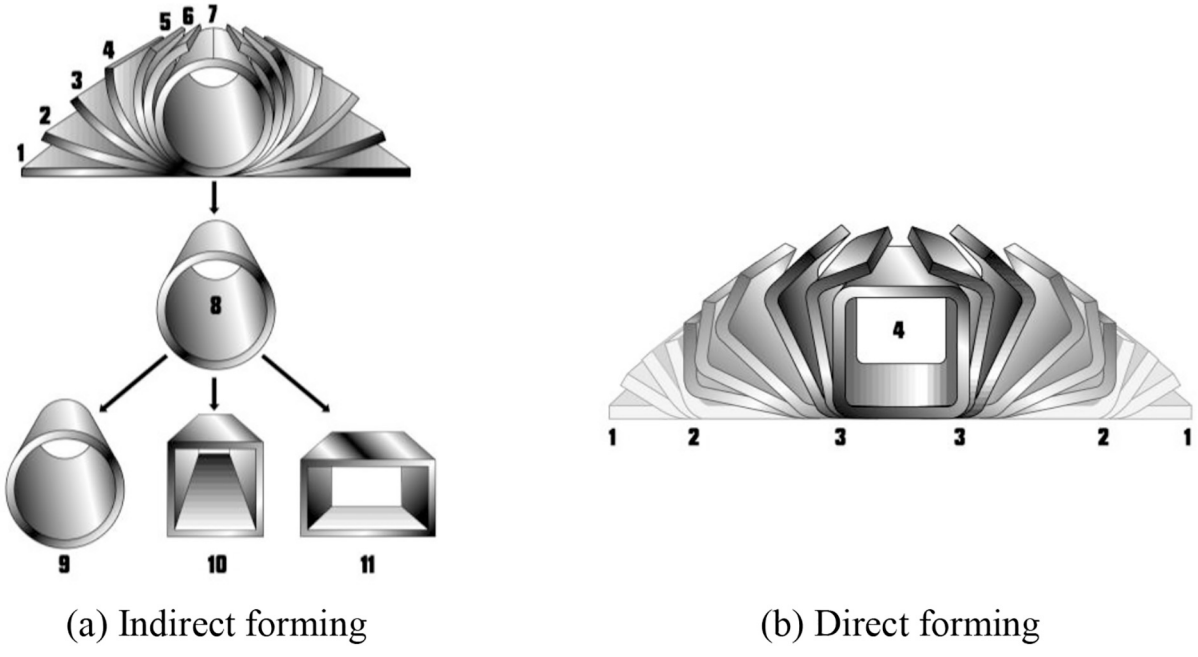

Fig. 1. Cold-forming methods.

strength RHS (untreated and galvanized) are examined using the experimental data.

2. Experimental investigation

2.1. Preparation of beam specimens

In this research, five regular-strength and five high-strength parent RHS are used to fabricate the beam specimens. For each parent RHS, half of the material is hot-dip galvanized and the other half remains untreated. The material properties of the untreated and galvanized RHS are obtained via tensile testing of coupons machined from flat faces and corners of the sections. The procedures and detailed discussions on the tensile testing can be found in [4]. The key tensile test results are listed in Table 1, where the RHS are given IDs with multiple components to differentiate material type, post-cold-forming process, and cross-sectional sizes. For the first component, D = direct-formed RHS (nominal yield stress = 350 MPa), and DH = direct-formed high-strength RHS (nominal yield stress = 690 MPa). For the second component, U = untreated, and G = galvanized. The third component gives the nominal width, depth, and thickness of the cross section (in mm). As shown in Table 1, post-production hot-dip galvanizing has minor effects on: (i) the ultimate strengths of the flat coupons; and (ii) the yield and ultimate strengths of the corner coupons. For the yield strengths of the flat coupons, an average increase of 8% is observed.

In a complimentary study [3], the residual stresses in 14 of the 20 RHS in Table 1 are measured using the sectioning method, where the measured values are resolved into membrane and bending components (σ_m and σ_b, respectively). For ease of discussions in the following sections of this paper, the key results are normalized by the measured yield stress (f_y) in Table 2, where the tensile membrane residual stresses are reported as positive values, and the compressive membrane residual stresses are reported as negative values. The tabulated bending residual stresses are the tensile residual stresses from the external surfaces of the RHS specimens. The bending residual stresses on the internal surfaces have the same magnitudes but opposite senses. As shown in Table 2, the application of post-production galvanizing can effectively lower the residual stress levels.

As shown in Table 3, the 20 RHS in Table 1 are used to produce a total of 22 beam specimens (including two additional specimens for repeated tests). Table 3 lists the measured cross-sectional dimensions including the average values of the measured flange external widths (B), web external depths (H), wall thicknesses (t) and internal corner radii (r). For measurement of internal corner radii, the RHS cross sections are scanned and input into AutoCAD where three-point arcs are drawn to fit the internal surfaces of all corners. The corner radii are obtained by measuring the radii of these arcs. The flange internal width-to-thickness ratios (b/t) and the web internal depth-to-thickness ratios (h/t) are also included in Table 3. It should be noted that all beam specimens are tested under bending about minor axes. Therefore, the flanges are the longer sides in all cases (Tables 1-3).

In AISC 360–16 [1], for flexural design of RHS, sections are designated as compact, noncompact or slender based on the width-to-thickness ratios of section elements under compression. Compact sections are capable of developing plastic moment and rotation capacity (R)

Table 2
Key residual stress measurement results.

RHS specimen	Flat		Corner		Overall	
	σ_b/f_y (%)	σ_m/f_y (%)	σ_b/f_y (%)	σ_m/f_y (%)	σ_b/f_y (%)	σ_m/f_y (%)
D-U-102 × 76 × 3.2	64	−35	45	16	62	−27
D-G-102 × 76 × 3.2	40	−8	27	2	38	−6
D-U-102 × 76 × 4.8	62	−6	29	11	56	−3
D-G − 102 × 76 × 4.8	37	-10	12	3	33	−8
D-U-102 × 102 × 4.8	88	−9	40	8	81	−7
DH-U-76 × 76 × 4.8	77	−5	35	11	69	−2
DH-G-76 × 76 × 4.8	41	−12	18	0	37	−10
DH-U-102 × 76 × 3.2	48	−17	33	19	46	−12
DH-G-102 × 76 × 3.2	25	−2	13	−2	24	−2
DH-U-102 × 76 × 4.1	54	−4	24	12	49	−2
DH-U-102 × 76 × 4.8	76	0	24	2	67	0
DH-G-102 × 76 × 4.8	37	−2	18	−3	34	−2
DH-U-152 × 76 × 4.1	52	−9	25	7	49	−7
DH-G-152 × 76 × 4.1	30	−10	10	6	27	−8

Table 1
Key tensile coupon test results.

RHS specimen	Flat coupons				Corner Coupons			
	E (GPa)	f_y (MPa)	f_u (MPa)	ε_{rup} (%)	E (GPa)	f_y (MPa)	f_u (MPa)	ε_{rup} (%)
D-U-102 × 76 × 3.2	203	367	492	34	200	601	672	14
D-G-102 × 76 × 3.2	211	400	509	32	208	599	664	16
D-U-102 × 76 × 4.8	200	409	470	39	217	568	605	18
D-G-102 × 76 × 4.8	204	424	463	36	225	574	595	20
D-U-102 × 102 × 3.2	203	344	469	32	220	567	623	15
D-G-102 × 102 × 3.2	198	380	497	32	223	536	638	15
D-U-102 × 102 × 4.8	205	399	487	38	206	574	618	18
D-G-102 × 102 × 4.8	219	470	515	30	218	596	620	20
D-U-127 × 127 × 4.8	202	395	457	40	213	553	588	16
D-G-127 × 127 × 4.8	200	427	468	37	223	574	603	22
DH-U-76 × 76 × 4.8	199	638	767	27	190	789	863	19
DH-G-76 × 76 × 4.8	203	743	786	28	229	878	893	22
DH-U-102 × 76 × 3.2	217	730	802	27	206	862	945	12
DH-G-102 × 76 × 3.2	217	742	803	20	207	876	904	14
DH-U-102 × 76 × 4.1	202	692	776	26	211	879	960	12
DH-G-102 × 76 × 4.1	202	711	792	26	227	901	909	17
DH-U-102 × 76 × 4.8	194	651	761	29	206	849	928	16
DH-G-102 × 76 × 4.8	191	720	777	26	225	816	876	20
DH-U-152 × 76 × 4.1	198	713	815	30	204	930	1054	14
DH-G-152 × 76 × 4.1	208	744	819	28	222	918	949	16

Table 3
Measured geometrical properties of RHS beam specimens.

Beam specimen	B (mm)	H (mm)	t (mm)	b/t	h/t	r (mm)	S ($\times 10^3$ mm^3)	Z ($\times 10^3$ mm^3)
D-U-102 × 76 × 3.2 D-G-102 × 76 × 3.2	101.9	76.5	3.03	29.6	21.2	2.4	25.5	29.3
D-U-102 × 76 × 4.8 D-G-102 × 76 × 4.8	101.9	76.4	4.36	19.4	13.5	3.4	34.3	40.2
D-U-102 × 102 × 3.2 D-G-102 × 102 × 3.2	101.9	101.1	3.03	29.6	29.4	3.4	36.8	42.8
D-U-102 × 102 × 4.8 D-G-102 × 102 × 4.8	102.1	101.6	4.4	19.2	19.1	5.6	50.9	60.1
D-U-127 × 127 × 4.8 D-G-127 × 127 × 4.8	127.6	127	4.4	25.0	24.9	6.6	82.5	96.4
DH-U-76 × 76 × 4.8 DH-G-76 × 76 × 4.8 DH-G-76 × 76 × 4.8(1)	76.3	76.6	4.81	11.9	11.9	8.5	28.8	34.8
DH-U-102 × 76 × 3.2 DH-U-102 × 76 × 3.2(1) DH-G-102 × 76 × 3.2	102.6	76.9	3.02	30.0	21.5	2.6	25.8	29.6
DH-U-102 × 76 × 4.1 DH-G-102 × 76 × 4.1	101.8	76.3	4.06	21.1	14.8	4.8	32.4	37.7
DH-U-102 × 76 × 4.8 DH-G-102 × 76 × 4.8	102	76.6	4.82	17.2	11.9	8.9	37.2	43.9
DH-U-152 × 76 × 4.1 DH-G-152 × 76 × 4.1	153.1	77.2	4.04	33.9	15.1	5.1	47.1	53.3

(1) Repeated test

of 3. Compact sections in AISC 360–16 [1] are equivalent to Class 1 sections in CSA S16–19 [2]. In AISC 360–16 [1], noncompact sections are defined as those capable of exceeding yield moment. Noncompact sections are equivalent to Class 2 and Class 3 sections in CSA S16–19 [2]. Sections not capable of developing yield moments (i.e., having elastic local buckling of elements in compression as the limit state) are designated as slender sections (or sections with slender elements) in AISC 360–16 [1] and Class 4 sections in CSA S16–19 [2]. For ease of evaluation of the existing slenderness limits in [1,2] in Section 4.1, the elastic and plastic section moduli based on the entire cross-sectional area are calculated using the measured dimensions and are listed in Table 3. In Section 4.2, for calculation of nominal flexural strengths of slender (Class 4) sections, using the effective width method in [1,2], the effective section moduli (S_e) are calculated considering the shift of neutral axes.

2.2. Beam tests

In this research, the beam specimens are tested under bending about their minor axes. This results in a complete range of flange local buckling behaviours (i.e., Classes 1, 2, 3 and 4 according to CSA S16–19 [2] or compact, noncompact and slender according to AISC 360–16 [1]). This allows for a comprehensive assessment of the flange slenderness limits and flexural design formulae in the existing standards [1,2]. Using the setup illustrated in Fig. 2, four-point bending tests are performed on the 22 direct-formed RHS beam specimens to study their flexural behaviours as well as the effects of post-production galvanizing and different strength grades. The beam specimens are simply supported at the two ends. Using a Tinius Olsen hydraulic testing machine with a capacity of 1000 kN and a spreader beam, a pair of concentrated forces are applied on each beam specimen at the two load application points to

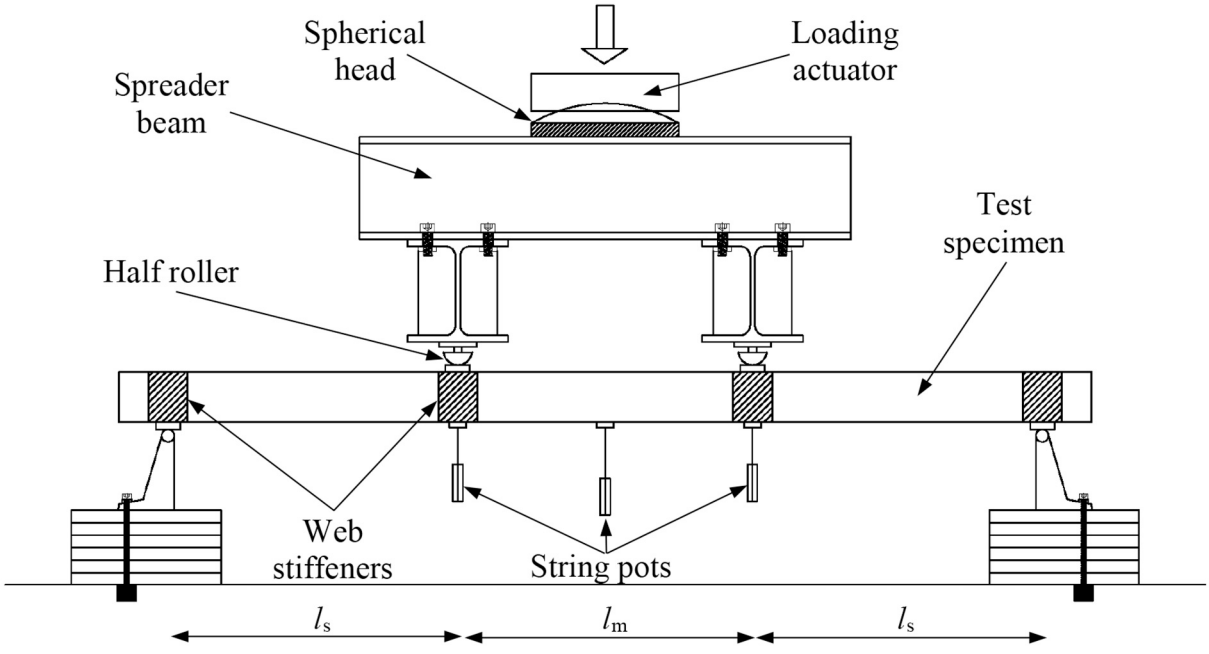

Fig. 2. Four-point bending test setup.

generate constant moment on the moment span. The moments are calculated using the recorded force data and the length of the shear span (L_s). String pots (with an accuracy of 0.01 mm) are installed at the locations of interest to record displacements, which are subsequently used to calculate curvature and rotation capacity of beam specimens. The beam specimens are loaded at a displacement rate of 2 mm/min. The loads and displacements are logged at one second intervals by the data acquisition system. All regular-strength RHS beam specimens have the same total length of 2 m and the same moment span length (L_m) of 0.6 m. All high-strength RHS beam specimens have the same total length of 1.4 m and the same moment span length of 0.4 m. In both cases, sufficient shear span lengths are provided to ensure that the sections fail by reaching their ultimate moment capacities before shear failures. To achieve the intended failure within the moment span, reinforcement (steel stiffeners and wood blocks in Fig. 3) is applied at load application points and supports to prevent unintended premature failure under concentrated forces.

With the test setup and the application of proper reinforcement, all 22 beam specimens reach their ultimate capacities by exhibiting failures between the two load application points (i.e., on moment span). Typical failures are shown in Fig. 4. Therefore, credence can be given to the test results.

2.3. Test results

The bending moments from the four-point bending tests (M) are normalized by the plastic moments ($M_p = Zf_y$) and plotted against normalized curvatures (κ/κ_p) in Fig. 5 for the regular- and high-strength RHS, where $\kappa_p = M_p/EI$ is the elastic curvature corresponding to M_p. The actual curvature of moment span (κ) is calculated using Eq. (1), where D_m is the deflection at the middle of moment span, and D_l is the average of the deflections at the two load application points [12]. The rotation capacities of the moment spans beam specimens are calculated using Eq. (2), where κ_u is curvature at plastic moment during unloading (Fig. 6). Such calculation approach is consistent with [1,2]. The calculated rotation capacities of all beam specimens are listed in Table 4 and will be used to evaluate: (i) the compact slenderness limit in AISC 360–16 [1] and (ii) the Class 1 slenderness limit from CSA S16–19 [2]. As discussed in Section 2.1, the other slenderness limits in [1,2] are based on section ultimate moment capacity (M_u). Therefore, the experimentally obtained M_u are normalized by the calculated M_y and M_p in Table 4. M_y and M_p are calculated using: (i) the measured yield strength of tensile coupons machined from flat faces of the RHS specimens, and (ii) the elastic and plastic section moduli in Table 3 based on the entire cross-sectional area of the RHS specimens. The key test results are listed in Table 4.

$$\kappa = \frac{8(D_m - D_l)}{4(D_m - D_l)^2 + L_m^2} \tag{1}$$

$$R = \frac{\kappa_u}{\kappa_p} - 1 \tag{2}$$

(a) D-U-76×102×4.8

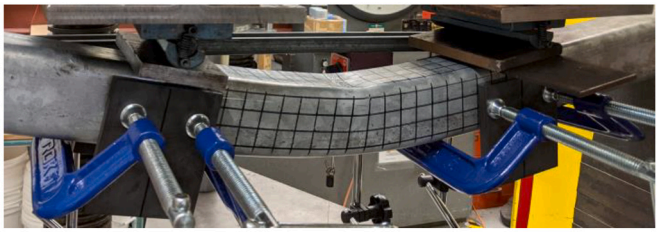

(b) DH-G-76×76×4.8

Fig. 4. Typical failures of beam specimens.

3. Flexural behaviours of sections with different production histories

This section presents a direct comparison of the flexural behaviours of RHS with similar cross-sectional dimensions and strength grades but different production histories (indirect-cold-formed versus direct-cold formed; cold-formed versus hot-finished; and untreated versus hot-dip galvanized). The applicability of the existing slenderness limits and flexural design formulae in the current North American steel design standards [1,2] is evaluated in Section 4.

The ultimate moment capacities of the indirect-cold-formed RHS (untreated) from [12,21–23] and the hot-finished RHS from [24,25] are shown in Fig. 7 for comparison to the direct-cold-formed RHS (untreated) from this research. For meaningful comparison, only the RHS from [12,21–25] with nominal yield stresses ranging from 350 to 700 MPa are selected. The ultimate moment capacities (M_u) are normalized by the corresponding plastic moments (M_p) calculated using the measured material and geometric properties and the approach discussed in Section 2. The normalized moment capacities are plotted against the normalized flange slenderness values $(b/t)\sqrt{f_y/E}$ (where b = internal flange width excluding corner portions; and E = Young's modulus). The moment capacities are not plotted against the normalized web slenderness values in this section. In this research, the flange slenderness values govern the cross-section classifications in all cases. Further

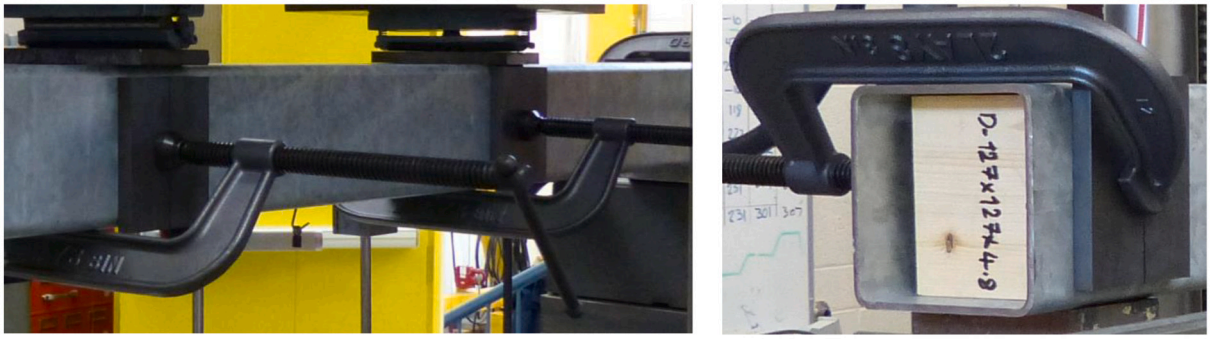

Fig. 3. Reinforcement at load application points and supports.

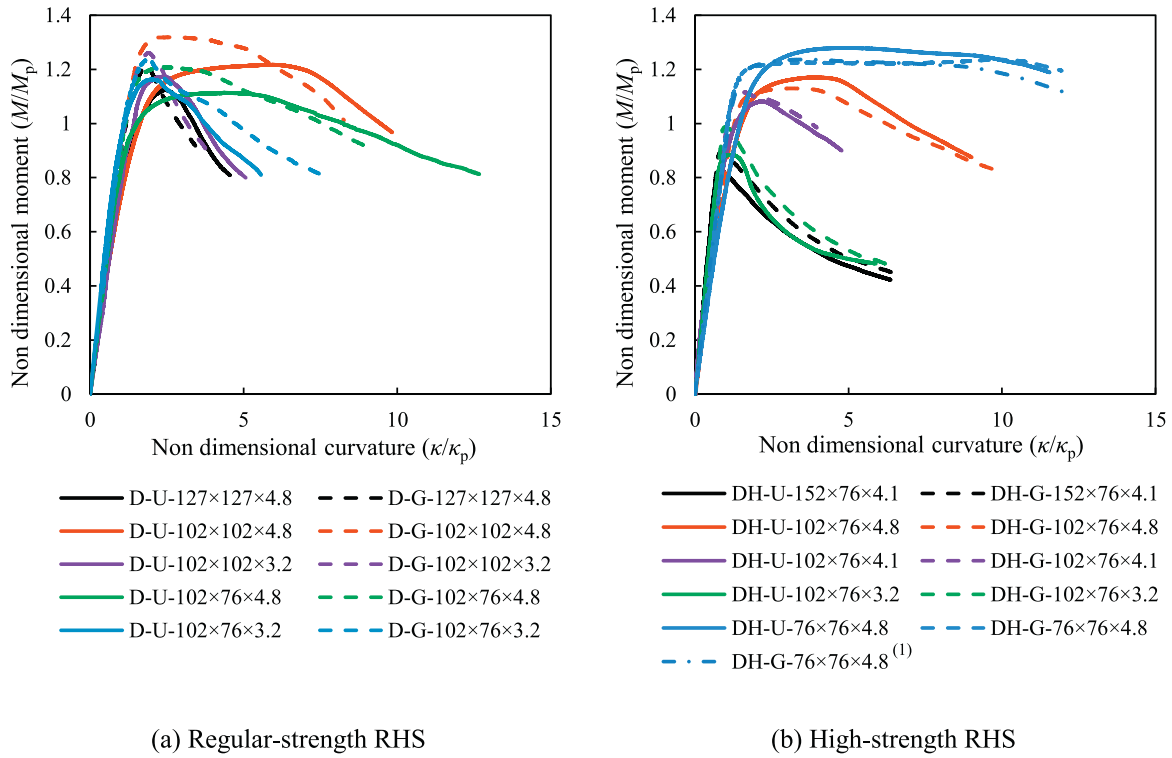

(a) Regular-strength RHS (b) High-strength RHS

Fig. 5. Normalized moment-curvature relationships of direct-formed RHS beam specimens.

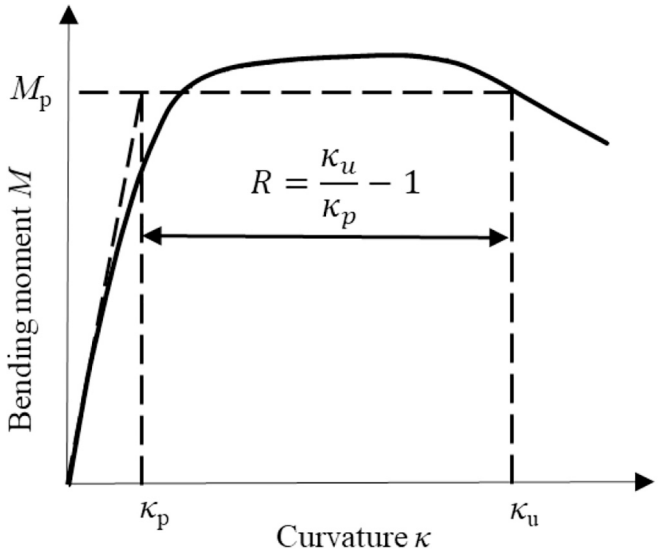

Fig. 6. Calculation of rotation capacity.

discussions on the cross-section classification rules and flexural design formulae relevant to both flanges and webs of RHS and built-up box sections are included in Section 4.

Associated with cold working is the development of high levels of residual stresses. The existence of high compressive residual stress (in RHS longitudinal direction) in general accelerates failure of compression flange in RHS under flexural loading. As illustrated in Fig. 1, the indirect-forming process roll-forms coil material into a CHS before further shaping it to an RHS. Therefore, the entire cross section has experience high degrees of cold working. Recent research involving measurement of residual stresses in 26 RHS specimens with different production histories [3] showed that, comparing to indirect-formed RHS, direct-formed RHS in general have lower levels of residual stresses since the cold-working is mainly concentrated at the four corner regions during production (Fig. 1). Therefore, it can be speculated that the compression flange in a direct-formed RHS can resist higher stress under flexural loading since the flat portion of the compression flange is not heavily cold-worked during production. Such speculation is substantiated by the comparison in Fig. 7a. As shown, in many cases the direct-formed RHS specimens have superior flexural strengths comparing to their indirect-formed RHS counterparts due to the delay of compression flange failure. This is consistent with the findings in [4,5] for stub column behaviours where the onsets of local buckling in direct-formed RHS are delayed considerably due to the inherently low levels of residual stresses.

As shown in Fig. 7b, over the range of flange slenderness values where previous experimental data [24,25] is available, the direct-cold-formed RHS specimens have superior flexural strengths comparing to the hot-finished RHS counterparts. It should be noted that the hot-finished RHS in [24,25] are produced by cold-forming coil material into CHS before hot-shaping it into RHS. The hot-shaping process (also know as hot-finishing) is performed at a normalizing temperature of approximately 900 °C. Such finishing intends to alter microstructure of steel, resulting in reduced hardness and increased ductility. Therefore, hot-finished products are excellent choices for applications such as dynamically loaded elements in welded structures, etc., where low-temperature notch-toughness properties may be important. It is also expected that all cold-forming-induced residual stresses are completely relieved at the normalizing temperature. However, as a trade-off, the cold-forming-induced strength enhancement is also removed, which explains the flexural strengths difference between the direct-cold-formed RHS specimens and the hot-finished RHS specimens in Fig. 7b.

Also shown in Figs. 7a an 7b are the existing flange slenderness limits for compact section from AISC 360–16 [1] and Class 2 section from CSA S16–19 [2]. In both cases, the sections are expected to reach the plastic moments (M_p). As shown, such flange slenderness limits are in general applicable for indirect-cold-formed and hot-finished RHS but

Table 4
Four-point bending test results.

Beam specimen	M_u (kNm)	M_y (kNm)	M_p (kNm)	M_u/M_y	M_u/M_p	R
D-U-102 × 76 × 3.2	12.5	9.4	10.8	1.34	1.17	3.1
D-G-102 × 76 × 3.2	13.3	9.4	10.8	1.42	1.24	4.2
D-U-102 × 76 × 4.8	18.3	14.0	16.4	1.30	1.11	6.6
D-G-102 × 76 × 4.8	19.8	14.0	16.4	1.41	1.21	6.0
D-U-102 × 102 × 3.2	17.1	12.7	14.7	1.35	1.16	1.6
D-G-102 × 102 × 3.2	18.4	12.7	14.7	1.45	1.25	2.8
D-U-102 × 102 × 4.8	29.0	20.3	24.0	1.43	1.21	7.1
D-G-102 × 102 × 4.8	29.9	20.3	24.0	1.47	1.25	5.8
D-U-127 × 127 × 4.8	42.1	32.6	38.1	1.29	1.11	1.5
D-G-127 × 127 × 4.8	45.5	32.6	38.1	1.40	1.20	1.5
DH-U-76 × 76 × 4.8	28.4	18.4	22.2	1.55	1.28	>9.6(2)
DH-G-76 × 76 × 4.8	27.5	18.4	22.2	1.50	1.24	>10.7(2)
DH-G-76 × 76 × 4.8(1)	27.5	18.4	22.2	1.50	1.24	>9.9(2)
DH-U-102 × 76 × 3.2	19.1	18.8	21.6	1.02	0.89	0.0(3)
DH-U-102 × 76 × 3.2(1)	19.2	18.8	21.6	1.02	0.89	0.0(3)
DH-G-102 × 76 × 3.2	21.3	18.8	21.6	1.13	0.99	0.0(3)
DH-U-102 × 76 × 4.1	28.3	22.4	26.1	1.26	1.08	2.0
DH-G-102 × 76 × 4.1	29.1	22.4	26.1	1.30	1.12	2.7
DH-U-102 × 76 × 4.8	33.4	24.2	28.6	1.38	1.17	4.2
DH-G-102 × 76 × 4.8	32.3	24.2	28.6	1.33	1.13	4.0
DH-U-152 × 76 × 4.1	31.5	33.6	38.0	0.94	0.83	0.0(3)
DH-G-152 × 76 × 4.1	34.3	33.6	38.0	1.02	0.90	0.0(3)

(1) Repeated test.
(2) Test stopped before moment reduced to M_p during unloading.
(3) Beam specimen did not reach M_p during loading.

conservative for direct-cold-formed RHS (untreated).

The comparisons of ultimate moment capacities of untreated and galvanized direct-formed RHS are shown in Fig. 8a and b for the regular- and high-strength materials, respectively. The following observations can be made:

(i) For regular-strength RHS, consistent increases of flexural strengths after hot-dip galvanizing are observed. This is consistent with the findings in the previous research on the effect of galvanizing on residual stresses in CHS [16] and RHS [3], where post-production galvanizing has been experimentally proven effective in partially relieving the cold-forming-induced residual stresses. The level of reduction is similar to the intended levels through the applications of post-production heat treatment per ASTM A1085 Supplement S1 [18], or the Class H finish per CSA G40.20/G40.21 [19] (both at 450 °C). Similar to such heat treatment, the molten zinc bath is typically maintained at 450 °C [3,16]. Such temperature does not alter grain structure and hence have minor effects on the material strengths. It can be seen in Fig. 8a that the existing flange slenderness limits for compact section from AISC 360–16 [1] and Class 2 section from CSA S16–19 [2] become even more conservative for galvanized direct-formed regular-strength RHS.

(ii) For high-strength RHS, increases of flexural strengths after hot-dip galvanizing are observed for sections with large slenderness values. On the other hand, no evident increase is observed for sections with small slenderness values based on the available experimental data in this study. It should be noted that all RHS specimens in this study are hot dipped in the same molten zinc bath at the same time for the same immersion duration. Therefore, there is no variation of thermal input among all RHS specimens. The RHS specimens with smaller slenderness values (corresponding to larger wall thicknesses in this research) have larger thermal masses. Therefore, for the same thermal input, the changes of residual stresses in them are smaller. In theory, the onset of local buckling is primarily affected by the residual stress-over-yield stress ratio. Therefore, it can be speculated that the galvanizing-induced improvement of flexural strengths would be smaller for high-strength RHS with large wall thicknesses, considering the smaller change of residual stress and high yield stress.

4. Comparisons to predictions by current North American flexural design rules

4.1. Cross-section slenderness limits

For flexural design, in AISC 360–16 [1] Table B4.1b, depending on the width-to-thickness ratios of the compression elements in members subject to flexure, steel sections are classified as compact, noncompact or slender. The slenderness limits for RHS and built-up box sections from [1] are reproduced here in Table 5, where the plastic slenderness limit (λ_p) differentiates compact and noncompact elements, and the yield slenderness limit (λ_r) differentiates noncompact and slender elements. After cross-section classification, the member nominal flexural strength can be calculated as the lowest values obtained according to the limit states of yielding (plastic moment), flange local buckling and web local buckling using the design formulae in Section F7 of AISC 360–16 [1]. Similarly, in CSA S16–19 [2] Table 1, depending on the width-to-thickness ratios of the compression elements in members subject to flexure, steel sections are classified as Class 1, 2, 3 or 4. The slenderness limits for RHS from [2] are reproduced here in Table 6, where λ_{c1}, λ_{c2} and λ_{c3} are the maximum slenderness values for Classes 1, 2 and 3. After cross-section classification, the member nominal flexural strength can be calculated using the design formulae in Section 13.5 of CSA S16–19 [2]. In this paper, Section 4.1 examines the applicability of the cross-section classification rules from AISC 360–16 [1] and CSA S16–19 [2] on direct-formed regular- and high-strength RHS (untreated and galvanized). Section 4.2 examines the applicability of the existing flexural design formulae in [1,2]. In this research, the cold-forming-induced strength enhancement (from flat fact to corner region) is captured by comparing the experimentally obtained flexural strengths to the calculated strengths. The calculated strengths are obtained using the design formulae from AISC 360–16 [1] and CSA S16–19 [2], and the measured yield stresses from the flat face coupons. The same methodology was applied in previous experimental and numerical studies on the flexural responses of cold-formed RHS beams [11,12,21].

The following observations can be made by comparing the slenderness limits in Tables 5 and 6:

(i) The plastic slenderness limits for compact sections from AISC 360–16 [1] ($\lambda_p = 1.12$ and 2.24 for flanges and webs in Table 5) and those for Class 1 sections from CSA S16–19 [2] ($\lambda_{c1} = 0.94$ and 2.46 for flanges and webs in Table 6) are slightly different. In design practice, actual corner radii are in general not available. Therefore, AISC 360–16 [8] calculates the internal width as external width minus 3 t, while CSA S16–19 [9] calculates

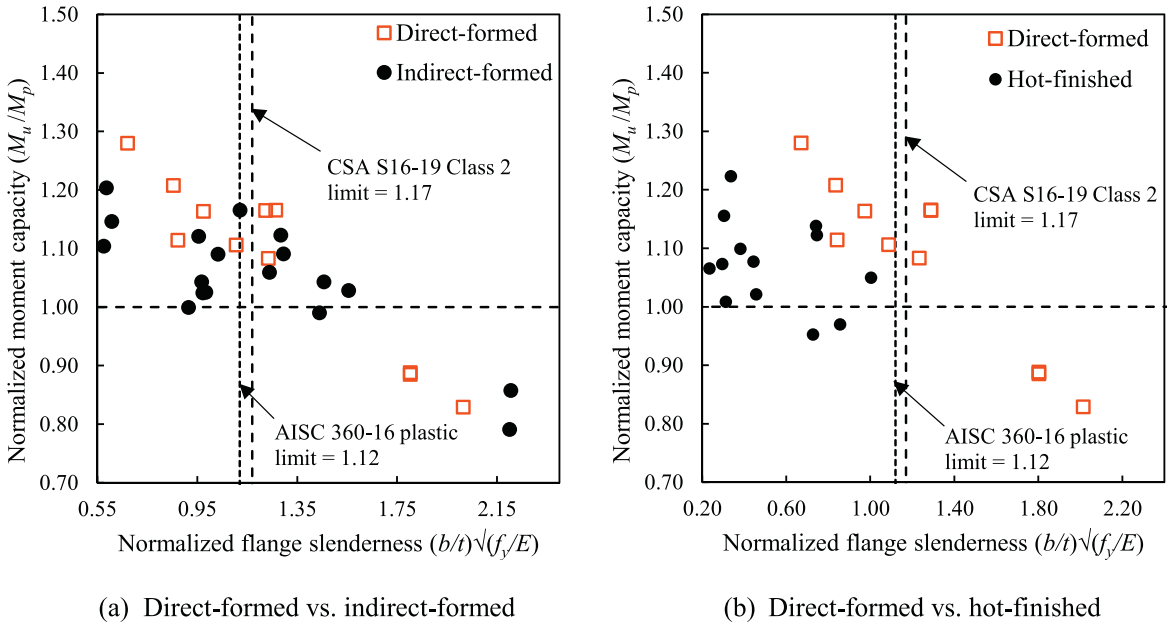

Fig. 7. Comparisons of direct-formed RHS (untreated) to indirect-formed RHS from [12,21–23] and hot-finished RHS from [24,25].

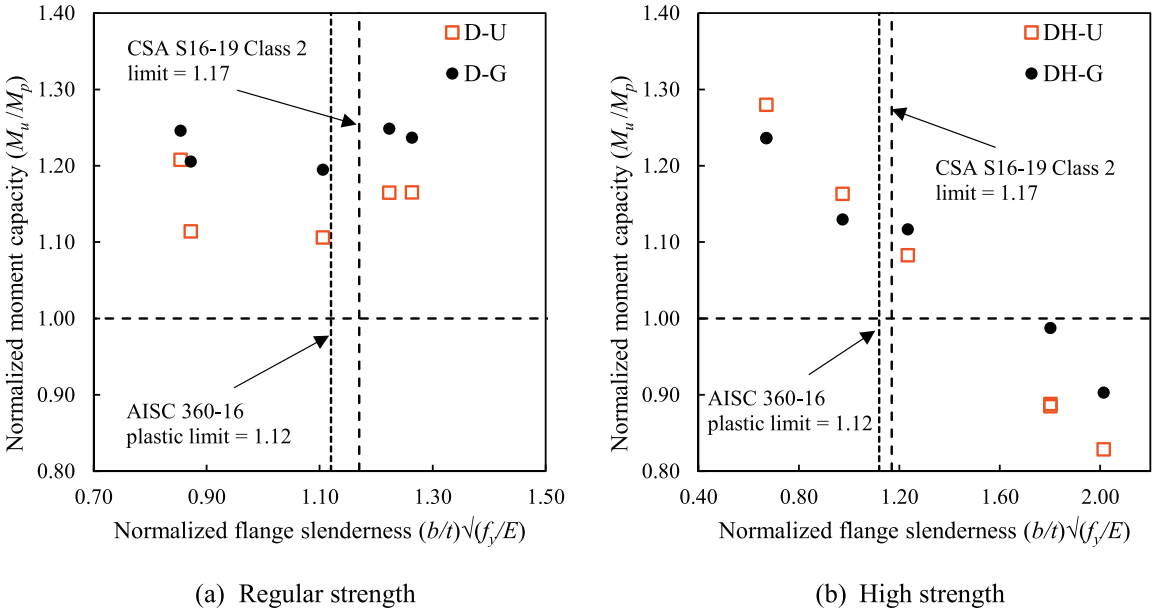

Fig. 8. Comparisons of untreated and galvanized direct-formed RHS.

Table 5
Slenderness limits for compression elements subject to flexure based on ANSI/AISC 360–16 [1].

Element description	Normalized slenderness	Normalized slenderness limits	
		λp	λr
Flanges of RHS	$(b/t)\sqrt{f_y/E}$	1.12	1.40
Webs of RHS and built-up box sections	$(h/t)\sqrt{f_y/E}$	2.42	5.70

Table 6
Slenderness limits for compression elements subject to flexure based on CSA S16–19 [9].

Element description	Normalized slenderness	Normalized slenderness limits		
		λ_{c1}	λ_{c2}	λ_{c3}
Flanges of RHS	$(b/t)\sqrt{f_y/E}$	0.94	1.17	1.50
Webs of RHS	$(h/t)\sqrt{f_y/E}$	2.46	3.80	4.25

internal width as external width minus 4 *t*. On the other hand, all section moduli in this research are calculated using the measured cross-sectional dimensions.

(ii) The flange slenderness limit for noncompact sections from AISC 360–16 [1] ($\lambda_r = 1.40$ in Table 5) and that for Class 3 sections from CSA S16–19 [2] ($\lambda_{c3} = 1.50$ in Table 6) are similar. However, the web slenderness limit for noncompact sections from AISC 360–16 [1] ($\lambda_r = 5.70$ in Table 5) is significantly more conservative than that for Class 3 sections from CSA S16–19 [2] ($\lambda_{c3} = 4.25$ in Table 6). In practice, for cold-formed RHS with commonly specified cross-sectional dimensions, flange slenderness usually governs the flexural behaviour. Therefore, $\lambda_r = 5.70$ in Table 5 caters mainly to built-up box sections with very small flange-width-to-web-depth ratios.

In AISC 360–16 [1] and CSA S16–19 [2], compact (Class 1) sections refer to those capable of developing plastic moments (M_P) and rotation capacity (R) of 3. Therefore, the rotational capacities of all RHS beam specimens (untreated and galvanized) are plotted against the normalized flange slenderness values in Fig. 9. The existing compact (Class 1) section slenderness limits for flanges (λ_p in Table 5 and λ_{c1} in Table 6) are also shown for direct comparison. Based on the best fit lines of the data points, both the AISC 360–16 [1] plastic limit and the CSA S16–19 [2] Class 1 limit are applicable. The applicability of the existing web slenderness limits cannot be evaluated (irrelevant) since the flange slenderness values govern the cross-section classifications of all RHS specimens in this research, which is often the case for flexural design of RHS with commonly specified (available) cross-sectional sizes. The same applies to the noncompact (Class 2 and Class 3) and slender (Class 4) RHS sections discussed herein.

In CSA S16–19 [2], Class 2 sections refer to those capable of developing plastic moments (M_P) but need not allow for subsequent moment redistribution. Therefore, for all RHS beam specimens (untreated and galvanized), the ultimate moment capacities (M_u) are normalized by the calculated plastic moments (M_P) and plotted against the normalized flange slenderness values in Fig. 10. The existing Class 2 section slenderness limits (λ_{c2} in Table 6) are also shown for direct comparison. The following observations can be made:

(i) Based on the best fit line for untreated direct-formed RHS in Fig. 10, the Class 2 flange slenderness limit from CSA S16–19 [2] is very conservative. A λ_{c2}-value of 1.50 may be more appropriate in this case. However, to propose accurate slenderness limit, a comprehensive FE parametric study is needed to produce more data points covering extended range of cross-sectional dimensions. As discussed in Section 1, comparing to the indirect-

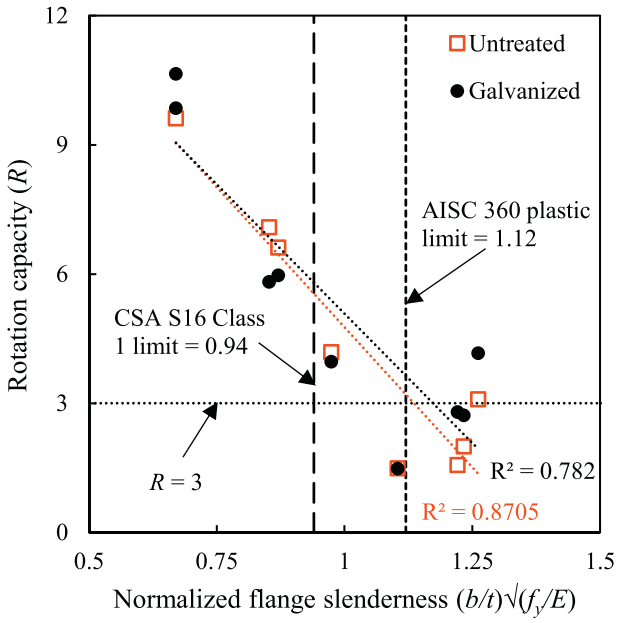

Fig. 9. Evaluation of Class 1 (plastic) flange slenderness limits in [1,2].

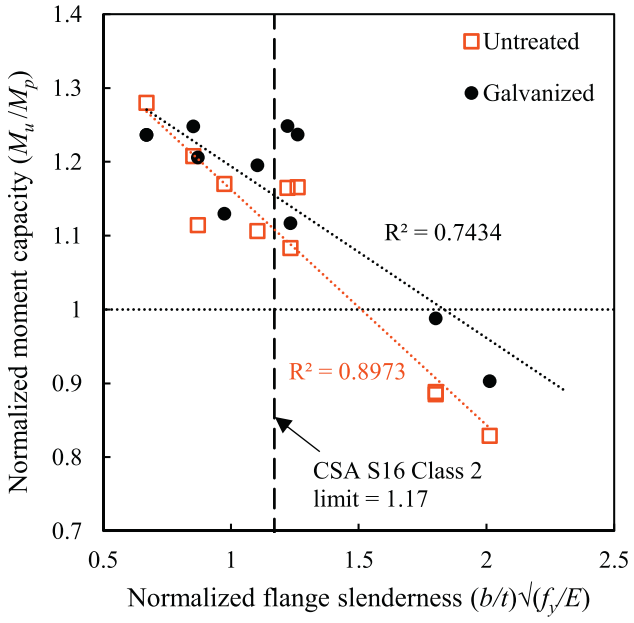

Fig. 10. Evaluation of Class 2 flange slenderness limits in [2].

forming approach, the direct-forming approach is relatively new. The existing cross-section classification rules for RHS in the North American steel design standards [1,2] were in general developed based on research on indirect-formed RHS. Since direct-formed RHS have inherently lower residual stress levels, it is intuitive that the existing flange slenderness limits can be conservative for them.

(ii) Based on the best fit line for galvanized direct-formed RHS in Fig. 10, the Class 2 flange slenderness limit from CSA S16–19 [2] becomes even more conservative. As discussed earlier, similar to the application of the heat treatment per ASTM A1085 Supplement S1 [18], or the Class H finish per CSA G40.20/G40.21 [19], the application of post-production galvanizing can effectively lower cold-forming-induced residual stresses (without removing the cold-forming-induced strength enhancement) and this in turn improves the member flexural behaviours. As shown, A λ_{c2}-value of 1.70 may be more appropriate for the flanges of the galvanized direct-formed RHS specimens.

In AISC 360–16 [1] and CSA S16–19 [2], noncompact (Class 3) sections refer to those capable of developing yield moments (M_y). Therefore, for all RHS beam specimens (untreated and galvanized), the ultimate moment capacities (M_u) are normalized by the calculated yield moments (M_y) and plotted against the normalized flange slenderness values in Fig. 14. The existing yield slenderness limit for noncompact (Class 3) sections (λ_r in Table 5 and λ_{c3} in Table 6) are also shown for direct comparison. The following observations can be made:

(i) Based on the best fit line for untreated direct-formed RHS in Fig. 11, both the AISC 360–16 [1] and CSA S16–19 [2] flange slenderness limits are very conservative. The existing yield (Class 3) slenderness limits (λ_r in Table 5 and λ_{c3} in Table 6) tend to misjudge nonslender sections as slender sections, since the inherently low levels of residual stresses in direct-formed RHS are not considered. This will result in unnecessary penalty and member strength underestimation when using the effective width method for flexural strength calculation. Based on the best fit line for untreated direct-formed RHS in Fig. 11, a λ_r (or λ_{c3})-value of 1.95 may be more appropriate for the flanges of the untreated direct-formed RHS specimens.

(ii) Similar to the comparisons between untreated and galvanized RHS specimens in Fig. 10, the codified yield (Class 3) slenderness limits become more conservative for the flanges of the galvanized direct-formed RHS specimens. A λ_r (or λ_{c3})-value of 2.25 may be more appropriate in this case.

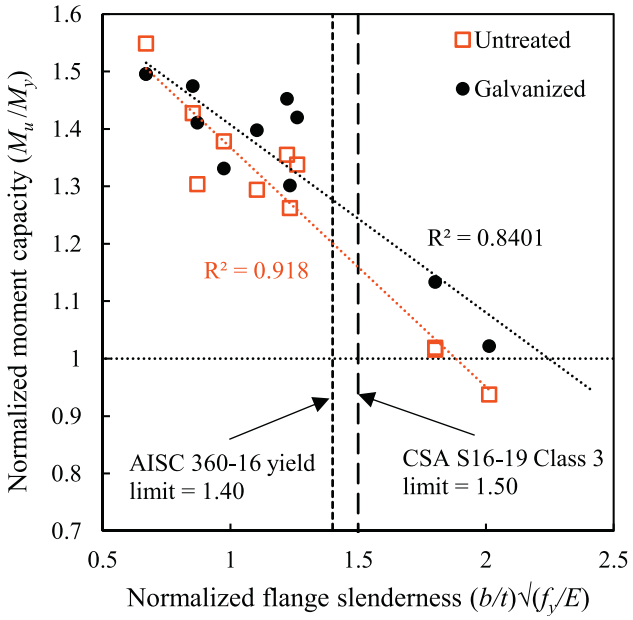

Fig. 11. Evaluation of Class 3 (yield) flange slenderness limits in [1,2].

As discussed in Section 3, for flexural design of cold-formed RHS of commonly specified (available) cross-sectional dimensions, the flange slenderness values usually govern the cross-section classifications, which is consistent with the RHS specimens in this experimental research and the commentaries in [1,2]. Therefore, the predicted cross-sectional behaviours based on the measured dimensions and the existing flange slenderness limits in Tables 5 and 6 from [1,2] are compared to the experimentally observed behaviours in Table 7. As shown, the existing slenderness limits from AISC 360–16 [1] and CSA S16–19 [2] are in many cases too conservative for direct-formed RHS (untreated and galvanized). Therefore, based on the available experimental data, this section has suggested some slenderness limits more suitable for direct-formed RHS (untreated and galvanized). However, a comprehensive FE parametric study is needed to cover extended ranges of cross-sectional dimensions to substantiate the suggested limits. It can also be seen in Table 7 (DH-U-152 × 76 × 4.1 versus DH-G-152 × 76 × 4.1) that the application of post-production galvanizing converted a slender section into a nonslender section in this study.

4.2. Flexural strengths

In this section, the experimentally obtained flexural strengths (i.e., ultimate moment capacities) are compared to the calculated nominal values (i.e., resistance factor = 1.00) to examine the flexural design formulae from AISC 360–16 [1] and CSA S16–19 [2].

In AISC 360–16 [1], for compact sections, the nominal flexural strengths equal the plastic moments. For sections with noncompact flanges and/or webs, two design formulae considering the limit states of flange local buckling and web local buckling are available. Both formulae provide linear transition from M_p to M_y, and M_n is determined as the lesser of the two. For design of sections with slender flange elements, AISC 360–16 [8] adopts the effective width approach, where effective section moduli (S_e) are calculated using effective flange widths (b_e) based on the λ_r-values in Table 5, considering the shift of neutral axis. AISC 360–16 Section F7.3 [8] contains formulae for calculation of nominal flexural strengths for sections with slender webs. However, this is an extremely rare case for cold-formed RHS with commonly specified cross-sectional dimensions. Such formulae in general cater to built-up box sections with very small flange-width-to-web-depth ratios. Therefore, such limit state and the corresponding design formulae are not evaluated in this section. In summary, for flexural design of RHS, the nominal strength shall be calculated as the lowest value obtained from Eqs. (3, 4, 6, 8) herein. As shown by Eqs. (5), (7) and (10), the flexural design formulae are heavily based on the existing slenderness limits in Table 5. As shown in Section 4.1, such limits are in many cases very conservative for direct-formed regular- and high-strength RHS

Table 7
Predicted and experimentally observed cross-sectional behaviours of beam specimens.

Beam specimen	$(b/t)\sqrt{f_y/E}$	Predicted behaviour based on [1,2]	Experimentally observed behaviour
D-U-102 × 76 × 3.2	1.26	Class 3 (noncompact)	Class 1 (compact)
D-G-102 × 76 × 3.2		Class 3 (noncompact)	Class 1 (compact)
D-U-102 × 76 × 4.8	0.87	Class 1 (compact)	Class 1 (compact)
D-G-102 × 76 × 4.8		Class 1 (compact)	Class 1 (compact)
D-U-102 × 102 × 3.2	1.22	Class 3 (noncompact)	Class 2 (noncompact)
D-G-102 × 102 × 3.2		Class 3 (noncompact)	Class 2 (noncompact)
D-U-102 × 102 × 4.8	0.85	Class 1 (compact)	Class 1 (compact)
D-G-102 × 102 × 4.8		Class 1 (compact)	Class 1 (compact)
D-U-127 × 127 × 4.8	1.11	Class 2 (compact)	Class 2 (noncompact)
D-G-127 × 127 × 4.8		Class 2 (compact)	Class 2 (noncompact)
DH-U-76 × 76 × 4.8	0.67	Class 1 (compact)	Class 1 (compact)
DH-G-76 × 76 × 4.8		Class 1 (compact)	Class 1 (compact)
DH-G-76 × 76 × 4.8(1)		Class 1 (compact)	Class 1 (compact)
DH-U-102 × 76 × 3.2	1.80	Class 4 (slender) with FLB (2)	Class 3 (noncompact)
DH-U-102 × 76 × 3.2(1)		Class 4 (slender) with FLB (2)	Class 3 (noncompact)
DH-G-102 × 76 × 3.2		Class 4 (slender) with FLB (2)	Class 3 (noncompact)
DH-U-102 × 76 × 4.1	1.23	Class 3 (noncompact)	Class 2 (noncompact)
DH-G-102 × 76 × 4.1		Class 3 (noncompact)	Class 2 (noncompact)
DH-U-102 × 76 × 4.8	0.97	Class 2 (compact)	Class 1 (compact)
DH-G-102 × 76 × 4.8		Class 2 (compact)	Class 1 (compact)
DH-U-152 × 76 × 4.1	2.01	Class 4 (slender) with FLB (2)	Class 4 (slender) with FLB (2)
DH-G-152 × 76 × 4.1		Class 4 (slender) with FLB (2)	Class 3 (noncompact)

(1) Repeated test.
(2) FLB = flange local buckling.

(untreated and galvanized). Therefore, it can be expected that the predicted nominal flexural strengths will be conservative as well.

Limit state: yielding of entire cross section

$$M_n = M_p = f_y Z \tag{3}$$

Limit state: flange local buckling for sections with noncompact flanges

$$M_n = M_p - (M_p - M_y)\left[3.57(b/t)\sqrt{f_y/E} - 4.0\right] \le M_p \tag{4}$$

Eq. (4) is derived using the following general formula (Eq. (5)):

$$M_n = M_p - (M_p - M_y)\left[\frac{(b/t)\sqrt{f_y/E} - \lambda_p}{\lambda_r - \lambda_p}\right] \le M_p \tag{5}$$

where $\lambda_p = 1.12$ and $\lambda_r = 1.40$ from Table 5.

Limit state: web local buckling for sections with noncompact webs

$$M_n = M_p - (M_p - M_y)\left[0.305(h/t)\sqrt{f_y/E} - 0.738\right] \le M_p \tag{6}$$

Eq. (6) is derived using the following general formula (Eq. (7)):

$$M_n = M_p - (M_p - M_y)\left[\frac{(h/t)\sqrt{f_y/E} - \lambda_p}{\lambda_r - \lambda_p}\right] \le M_p \tag{7}$$

where $\lambda_p = 2.42$ and $\lambda_r = 5.70$ from Table 5.

Limit state: flange local buckling for sections with slender flanges

$$M_n = f_y S_e \tag{8}$$

where S_e = effective section modulus determined with the effective width, b_e, of the compression flange taken as:

$$b_e = \begin{cases} b \text{ when } (b/t)\sqrt{f_y/E} \le 1.40 \\ 1.92t\sqrt{E/f_y}\left(1 - \dfrac{0.38\sqrt{E/f_y}}{b/t}\right) \text{ when } (b/t)\sqrt{f_y/E} > 1.40 \end{cases} \tag{9}$$

Eq. (9) is derived using the following general formula (Eq. (10)):

$$b_e = \begin{cases} b \text{ when } (b/t)\sqrt{f_y/E} \le \lambda_r \\ \left[\dfrac{c_2\lambda_r}{(b/t)\sqrt{f_y/E}} - c_1\left(\dfrac{c_2\lambda_r}{(b/t)\sqrt{f_y/E}}\right)^2\right] b \text{ when } (b/t)\sqrt{f_y/E} > \lambda_r \end{cases} \tag{10}$$

where $c_1 = 0.2$ and $c_2 = 1.38$ are the effective width imperfection adjustment factors from Table E7.1 in AISC 360–16 [1]. $\lambda_r = 1.40$ is from Table 5.

In CSA S16–19 [2], for Class 1 and Class 2 RHS sections, $M_n = M_p = f_y Z$. For Class 3 RHS sections $M_n = M_y = f_y S$. For Class 4 RHS sections with slender webs, similar to the approach in AISC 360–16 [1], effective section moduli (S_e) are determined using an effective flange width of $670\ t/\sqrt{f_y}$ (based on the Class 3 slenderness limit in Table 6), considering the shift of neutral axes, and $M_n = M_y = f_y S_e$. Calculation rule is available for sections with flanges meeting the requirements of Class 3 but the web slenderness exceeding the limit for Class 3. However, such calculation rule in general cater to built-up box sections with very small flange-width-to-web-depth ratios and is thus not applicable to cold-formed RHS with commonly specified cross-sectional dimensions.

The experimentally obtained ultimate moment capacities (M_u) of the RHS beam specimens are compared to the design curves based on the formulae in [1,2] in Figs. 12 and 13. The key statistics of the comparisons between M_u and the nominal flexural strengths calculated based on [1,2] ($M_{u,AISC}$ and $M_{u,CSA}$, respectively) are listed in Table 8. The following observations can be made:

(i) As shown in Figs. 12 and 13, in all cases the predictions by AISC 360–16 [1] and CSA S16–19 [2] are conservative for direct-formed regular- and high-strength RHS (untreated and galvanized). CSA S16–19 [2] is slightly more conservative based on the average M_u/M_n-ratios in Tables 8 and 9.
(ii) For the RHS specimens classified as compact (Class 1) sections based on the existing slenderness limits, both AISC 360–16 [1] and CSA S16–19 [2] provide conservative predictions for flexural strengths (Figs. 12 and 13) since the cold-forming-induced strength enhancements above f_y are not considered in calculation.
(iii) For the RHS specimens classified as noncompact (Class 2 and Class 3) sections based on the existing slenderness limits, both AISC 360–16 [1] and CSA S16–19 [2] provide conservative predictions (Figs. 12 and 13) since the inherently low levels of residual stresses in direct-formed RHS are not considered. AISC 360–16 [1] provides better predictions since a linear transition from M_p to M_y is considered for noncompact sections.

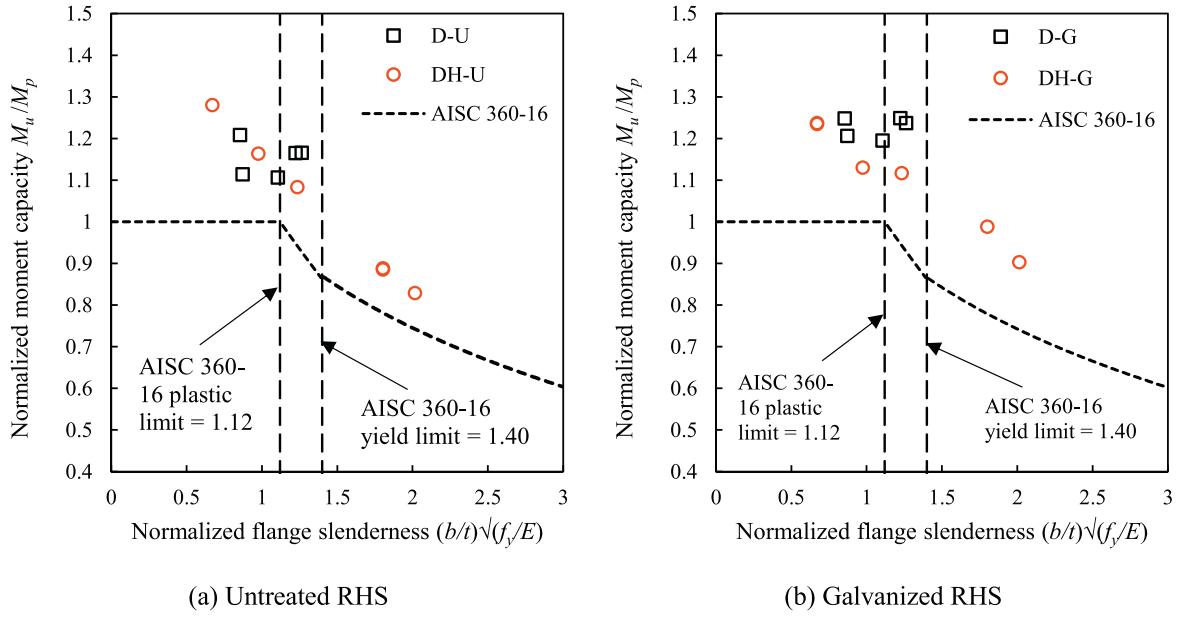

Fig. 12. Comparisons of experimental results with nominal flexural strengths calculated using AISC 360–16 [1].

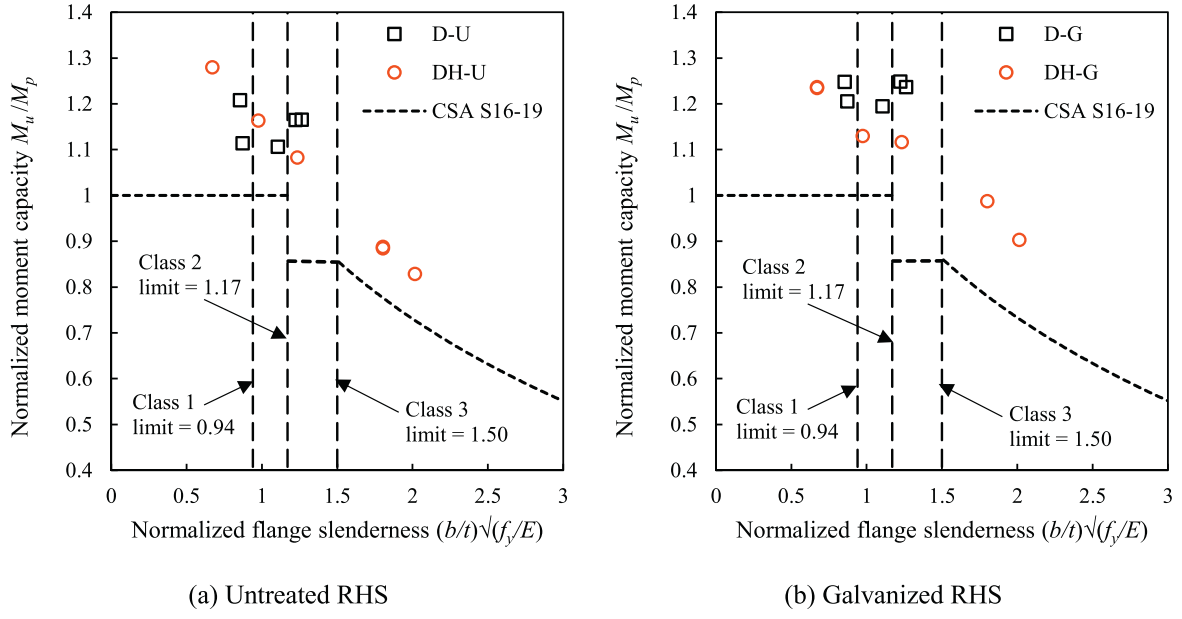

Fig. 13. Comparisons of experimental results with nominal flexural strengths calculated using CSA S16–19 [2].

Table 8
Key comparison results for untreated direct-formed RHS beam specimens.

Beam specimen	M_u (kN.m)	M_u / $M_{n,AISC}$	M_u / $M_{n,CSA}$
D-U-102 × 76 × 3.2	12.5	1.21	1.29
D-U-102 × 76 × 4.8	18.3	1.19	1.19
D-U-102 × 102 × 3.2	17.1	1.15	1.22
D-U-102 × 102 × 4.8	29.0	1.26	1.26
D-U-127 × 127 × 4.8	42.1	1.14	1.14
DH-U-76 × 76 × 4.8	28.4	1.19	1.19
DH-U-102 × 76 × 3.2	19.1	1.19	1.19
DH-U-102 × 76 × 3.2(1)	19.2	1.19	1.20
DH-U-102 × 76 × 4.1	28.3	1.16	1.27
DH-U-102 × 76 × 4.8	33.2	1.11	1.11
DH-U-152 × 76 × 4.1	31.5	1.15	1.18
Mean (D—U)		1.19	1.22
COV (D—U)		0.041	0.048
Mean (DH-U)		1.17	1.19
COV (DH-U)		0.028	0.043
Mean (D-U + DH-U)		1.18	1.20
COV (D-U + DH-U)		0.034	0.043

(1) Repeated test

Table 9
Key comparison results for galvanized direct-formed RHS beam specimens.

Beam specimen	M_u (kN.m)	M_u / $M_{n,AISC}$	M_u / $M_{n,CSA}$
D-G-102 × 76 × 3.2	12.5	1.29	1.36
D-G-102 × 76 × 4.8	18.3	1.29	1.29
D-G-102 × 102 × 3.2	17.1	1.23	1.31
D-G-102 × 102 × 4.8	29.0	1.30	1.30
D-G-127 × 127 × 4.8	42.1	1.24	1.24
DH-G-76 × 76 × 4.8	28.4	1.15	1.15
DH-G-76 × 76 × 4.8(1)	19.1	1.15	1.15
DH-G-102 × 76 × 3.2	19.2	1.32	1.33
DH-G-102 × 76 × 4.1	28.3	1.19	1.31
DH-G-102 × 76 × 4.8	33.2	1.07	1.07
DH-G-152 × 76 × 4.1	31.5	1.25	1.29
Mean (D-G)		1.27	1.30
COV (D-G)		0.026	0.033
Mean (DH-G)		1.19	1.22
COV (DH-G)		0.073	0.088
Mean (D-G + DH-G)		1.23	1.26
COV (D-G + DH-G)		0.060	0.069

(1) Repeated test

(iv) For the RHS specimens classified as slender (Class 4) sections based on the existing slenderness limits, both AISC 360–16 [1] and CSA S16–19 [2] provide conservative predictions. As shown in Figs. 12 and 13, the existing design curves have the tendency to misjudge nonslender direct-formed sections as slender sections, resulting in unnecessary penalty to effective cross-sectional area and underestimation of flexural strengths.

(v) Based on available data and the average M_u/M_n-ratios in Tables 8 and 9, it can be seen that: (a) the existing design provisions are more conservative for galvanized RHS than untreated RHS; and (b) the existing design provisions are more conservative for regular-strength RHS than high-strength RHS.

(vi) Based on the above, it will be desirable to use the experimental results from the 22 full-scale beam tests to develop and validate FE models for a comprehensive parametric study to produce more data points covering extended ranges of cross-sectional dimensions. A reliability analysis can then be performed to accurately assess the applicability of existing design rules and propose modified design rules as necessary.

5. Conclusions

In this paper, the flexural behaviours of new-generation direct-formed RHS (nominal yield stresses of 350 and 690 MPa) are examined for the first time via a comprehensive testing program including a total of 22 full-scale beam specimens. The direct-formed RHS specimens are shown to have superior flexural behaviours by comparison to the indirect-cold-formed and hot-finished RHS specimens from previous studies. The application of post-production hot-dip galvanizing is proven effective in partially relieving cold-forming-induced residual stresses and improving the flexural behaviours of the direct-formed RHS specimens. The applicability of the flexural design rules in the current North American steel design standards on direct-formed regular- and high-strength RHS (untreated and galvanized) is evaluated using the experimental data. Based on the available test results, the limiting width-to-thickness ratio for noncompact RHS flange element (i.e., yield slenderness limit) in AISC 360–16 is found to be conservative for direct-formed RHS (ungalvanized and galvanized). Similarly, the Class 2 and Class 3 flange slenderness limits from CSA S16–19 are found to be conservative for direct-formed RHS (ungalvanized and galvanized). The flexural design formulae from both AISC 360–16 and CSA S16–19 produce conservative predictions for direct-formed RHS (ungalvanized and galvanized).

Declaration of Competing Interest

None.

Acknowledgements

The authors are grateful for the financial support from the Natural Sciences and Engineering Research Council of Canada (NSERC) and the British Columbia Institute of Technology (BCIT). Appreciation is extended to Bull Moose Tube and Silver City Galvanizing for their donation of material and service.

References

[1] ANSI/AISC, Specification for structural steel buildings, ANSI/AISC 360–16, American Institute of Steel Construction, Chicago-Illinois, Chicago, IL, USA, 2016.
[2] CSA, Limit States Design in Structural Steel, CSA S16–19, Canadian Standard association, Toronto, ON, Canada, 2019.
[3] K. Tayyebi, M. Sun, K. Karimi, Residual stresses of heat-treated and hot-dip galvanized RHS cold-formed by different methods, J. Constr. Steel Res. 169 (2020) 106071.
[4] K. Tayyebi, M. Sun, Stub column behaviour of heat-treated and galvanized RHS manufactured by different methods, J. Constr. Steel Res. 166 (2020) 105910.
[5] K. Tayyebi, M. Sun, Design of direct-formed square and rectangular hollow section stub columns, J. Constr. Steel Res. 178 (2021) 106499.
[6] ASTM, Standard Specification for Cold-Formed Welded High Strengh Carbon Steel or High-Strength Low-Allou Steel Hollow Structural Sections (HSS) in Rounds and Shapes, ASTM A1112/A1112M-18, American Society for Testing and Materials, West Conshohocken, PA, USA, 2018.
[7] X.L. Zhao, A. Heidarpour, L. Gardner, Recent developments in high-strength and stainless steel tubular members and connections, Steel Constr. 7 (2014) 65–72.
[8] T.M. Chan, X.L. Zhao, B. Young, Cross-section classification for cold-formed and built-up high strength carbon and stainless steel tubes under compression, J. Constr. Steel Res. 106 (2015) 289–295.
[9] J.L. Ma, T.M. Chan, B. Young, Material properties and residual stresses of cold-formed high strength steel hollow sections, J. Constr. Steel Res. 109 (2015) 152–165.
[10] J.L. Ma, T.M. Chan, B. Young, Experimental investigation on stub-column behavior of cold-formed high-strength steel tubular sections, J. Struct. Eng. 142 (2016), 04015174.
[11] J.L. Ma, T.M. Chan, B. Young, Design of cold-formed high-strength steel tubular stub columns, J. Struct. Eng. 144 (2018), 04018063.
[12] J.L. Ma, T.M. Chan, B. Young, Experimental investigation of cold-formed high strength steel tubular beams, Eng. Struct. 126 (2016) 200–209.
[13] J.L. Ma, T.M. Chan, B. Young, Design of cold-formed high strength steel tubular beams, Eng. Struct. 151 (2017) 432–443.
[14] J. Wang, S. Afshan, N. Schillo, M. Theofanous, M. Feldmann, L. Gardner, Material properties and compressive local buckling response of high strength steel square and rectangular hollow sections, Eng. Struct. 130 (2017) 297–315.
[15] X. Lan, J. Chen, T.M. Chan, B. Young, The continuous strength method for the design of high strength steel tubular sections in compression, Eng. Struct. 162 (2018) 177–187.
[16] G. Shi, X. Jiang, W. Zhou, T.M. Chan, Y. Zhang, Experimental investigation and modeling on residual stress of welded steel circular tubes, Int. J. Steel Struct. 13 (2013) 495–508.
[17] M. Sun, Z. Ma, Effects of heat-treatment and hot-dip galvanizing on mechanical properties of RHS, J. Constr. Steel Res. 153 (2019) 603–617.

[18] ASTM, Standard Specification for Cold-Formed Welded Carbon Steel Hollow Structural Sections (HSS), ASTM A1085/A1085M-15, American Society for Testing and Materials, West Conshohocken, PA, USA, 2015.
[19] CSA, General requirements for rolled or welded structural quality steel / Structural quality steel, CSA G40.20–13/G40.21–13, Canadian Standards Association, Toronto, Canada, 2013.
[20] M. Sun, J.A. Packer, Hot-dip galvanizing of cold-formed steel hollow sections: a state-of-the-art review, Front. Struct. Civ. Eng. 13 (2019) 49–65.
[21] L. Gardner, N. Saari, F. Wang, Comparative experimental study of hot-rolled and cold-formed rectangular hollow sections, Thin-Walled Struct. 48 (2010) 495–507.
[22] T. Wilkinson, G.J. Hancock, Tests to examine compact web slenderness of cold-formed RHS, J. Struct. Eng. 124 (1998) 1166–1174.
[23] X. Zhao, G.J. Hancock, Square and rectangular hollow sections subject to combined actions, J. Struct. Eng. 118 (1992) 648–667.
[24] J. Wang, S. Afshan, M. Gkantou, M. Theofanous, C. Baniotopoulos, L. Gardner, Flexural behaviour of hot-finished high strength steel square and rectangular hollow sections, J. Constr. Steel Res. 121 (2016) 97–109.
[25] X. Meng, L. Gardner, Testing of hot-finished high strength steel SHS and RHS under combined compression and bending, Thin-Walled Struct. 148 (2020) 106262.